

A search for a contribution from axion-like particles to the X-ray diffuse background utilizing the Earth's magnetic field

R. Yamamoto,^{a,1} N.Y. Yamasaki,^a K. Mitsuda^a and M. Takada^b

^aInstitute of Space and Astronautical Science,
3-1-1, Yoshinodai, Chuo-ku, Sagami-hara, Kanagawa, Japan

^bKavli Institute for the Physics and Mathematics of the Universe, University of Tokyo,
5-1-5, Kashiwanoha, Kashiwa, Chiba, Japan

E-mail: r.yamamoto@aist.go.jp, yamasaki@astro.isas.jaxa.jp,
mitsuda@astro.isas.jaxa.jp, masahiro.takada@ipmu.jp

Received June 12, 2019

Revised October 21, 2019

Accepted December 3, 2019

Published February 11, 2020

¹Corresponding author. Present address: Advanced Institute for Science and Technology, 1-1-1, Umezono, Tsukuba, Ibaraki, Japan



Abstract. The Axion Like Particle (ALP) is a hypothetical pseudo-scalar particle beyond the Standard Model, with a compelling possible connection to dark matter and early universe physics. ALPs can be converted into photons via interactions with magnetic fields in the universe, i.e., the so-called inverse Primakoff effect. In this paper, we propose a novel method to explore ALP-induced photons from X-ray data obtained from the *Suzaku* satellite, arising from a possible interaction of ALPs with the direction-dependent Earth’s magnetic field viewed from the satellite. *Suzaku* data is suitable for this purpose because its low-altitude Earth orbit result in intrinsically low cosmic-ray background radiation. We study whether the X-ray diffuse background (XDB) spectra estimated from the four deep fields collected over eight years, vary with the integrated Earth’s magnetic strength in the direction of each target field at each observation epoch, which amounts to 10^2 Tm — a value greater than that achieved by terrestrial experiments due to the large coherent length. From the detailed analysis, we did not find evidence of the XDB confidence level spectra having dependence on the Earth’s magnetic strength. We obtained 99% confidence level upper limit on a possible residual contribution to the cosmic X-ray background (CXB) surface brightness to be 1.6×10^{-9} ergs s $^{-1}$ cm $^{-2}$ sr $^{-1}$ normalized at 10^4 T 2 m 2 in the 2–6 keV range, which corresponds to 6–15% of the observed CXB brightness, depending on which model of unresolved point sources are used in the interpretation. It is consistent with 80–90% of the CXB now being resolved into point sources.

Keywords: axions, X-rays, X-ray telescopes

ArXiv ePrint: [1906.04429](https://arxiv.org/abs/1906.04429)

Contents

1	Introduction	1
2	Process of photon emission from ALPs	2
3	Analysis and results: a search for the correlation between residual <i>Suzaku</i> background radiation with the Earth's magnetic strength	4
3.1	Selection of blank sky observations from <i>Suzaku</i> archival data	4
3.2	An assessment of non-Xray background contamination	6
3.3	Spectral analysis for $(B_{\perp}L)^2$ sorted data	8
4	Discussion and conclusions	11

1 Introduction

Various cosmological observations have provided strong evidence for the existence of dark matter. However, if dark matter is to be an elementary particle, it is a yet-unknown particle beyond the Standard Model. The Axion-Like Particle (ALP) is a hypothetical pseudo-scalar particle beyond the Standard Model, and is a consequence of the quantum field for conserving CP symmetry in the strong interaction [1, 2]. ALPs are attractive because they act like cold dark matter (CDM) in the formation of cosmic structure. It is possible that ALPs are created by a decay of other CDM-candidate particles. If ALP mass is too low, a direct experiment with present techniques is unlikely to find it. A possible channel is to observe photons, which are created by ALPs following the inverse Primakoff process in an electromagnetic field. As we show in detail in section 2, the ALP-photon conversion probability $P_{a \rightarrow \gamma}$ is approximately proportional to the squared product of magnetic field strength orthogonal to the ALP momentum direction, B_{\perp} , and the length, L , i.e., $P_{a \rightarrow \gamma} \propto (B_{\perp}L)^2$.

There have been many attempts to detect ALP signals in terrestrial experiments and astronomical observations. One candidate signal is in the direction of galaxies or galaxy clusters, which was proposed to be due to ALP interaction with inter-stellar or galactic magnetic fields [3–5], although the results are still under discussion. If ALPs are CDM itself or produced from a decay of CDM at cosmological distances and if those can be observed, the distribution of ALPs or ALP-induced photons via its interaction with magnetic fields in cosmic structures should appear to be isotropic in the sky to the zero-th order approximation, unless we have high-sensitivity and high-angular resolution data to resolve the distribution tracing inhomogeneous cosmic structures in the universe.

In this paper, we propose a novel method to search for ALP-induced photons from the satellite X-ray data, arising from the Primakoff interaction of the ALPs with the Earth's magnetic field. The Earth's magnetic field is known to have a dipole structure around the Earth in a north-south direction and we have a good knowledge of its strength and field configuration from various observations. Therefore, we can expect the ALP-induced photons in X-ray wavelengths, if produced, to vary with the Earth's magnetic field strength integrated along the line-of-sight direction for each observation, even if ALPs arriving on Earth have an isotropic distribution in the sky. To search for such ALP-origin X-ray radiation, we focus on the *Suzaku* X-ray data in the four deep fields, collected over eight years. These fields had

been observed frequently by the *Suzaku*, but the magnetic field strengths varied with each observation depending on its location in the orbit. For a null hypothesis of ALP-induced photons, the diffuse X-ray background brightness estimated from the same field should *not* show any dependence on the integrated magnetic field. This is the signal we will search for in this paper. *Suzaku* data is suitable for our purpose, because the satellite, compared to the *XMM-Newton*¹ or *Chandra*,² has lower background due to its low-altitude orbit that prevents cosmic rays from penetrating the X-ray detectors [6].

Our study is somewhat similar to Fraser et al., (2014) [7], which claimed a detection of seasonal variations in the *XMM-Newton* X-ray data. The work claimed that the X-ray flux modulation at a level $4.6 \times 10^{-12} \text{ ergs s}^{-1} \text{ cm}^{-2} \text{ deg}^{-2}$ in 2–6 keV might be due to a conversion of solar axions by their interaction with the Earth’s magnetic field (also see [8, 9]). However, Roncadelli and Tavecchio, (2015) [10] claimed that the *XMM-Newton* satellite which never points toward the Sun cannot observe such ALP-induced photons originating from solar axions due to momentum conservation.

The structure of this paper is as follows. In section 2, we briefly review basics of the inverse Primakoff effect and how photons can be induced by the effect from ALPs that are created by dark matter in the expanding universe. In section 3 we show the main results of this paper using the *Suzaku* data, when combined with data of the Earth’s magnetic field at each orbit of the *Suzaku* satellite at each observation. Section 4 contains the discussion and conclusion.

2 Process of photon emission from ALPs

In this section we describe a mechanism of photon emission from ALPs via the interaction with magnetic fields. To do this, we consider a model in which dark matter, which fills up space of the universe, preferentially decays into ALPs. This model is an example of moduli dark matter model in a string-theory-inspired scenario.

When a dark matter particle decays into two ALPs, i.e. $\text{DM} \rightarrow 2\text{ALPs}$, each ALP has a monochromatic energy $E_a = m_\phi/2$, where m_ϕ is the mass of the dark matter particle. The emissivity of $\text{DM} \rightarrow 2\text{ALPs}$ decaying process is given in terms of the energy density of dark matter, $\rho_\phi(r)$, the decay rate, $\Gamma_{\phi \rightarrow 2a}$, and m_ϕ as

$$\epsilon_a = \frac{2\rho_\phi(r) \Gamma_{\phi \rightarrow 2a}}{m_\phi}. \quad (2.1)$$

Considering the spatial distribution of dark matter along the line-of-sight direction, the ALP intensity, $I_{a,\text{line}}$ [counts $\text{s}^{-1} \text{ cm}^{-2} \text{ sr}^{-1}$], is given as

$$I_{a,\text{line}} = \int_{\text{l.o.s.}} \frac{2\Gamma_{\phi \rightarrow 2a}}{4\pi m_\phi} \rho_\phi(r) dr = \frac{S_\phi \Gamma_{\phi \rightarrow 2a}}{2\pi m_\phi}, \quad (2.2)$$

at $E_a = m_\phi/2$, and S_ϕ is the column density of dark matter in the line-of-sight direction [11], defined as

$$S_\phi = \int_{\text{l.o.s.}} \rho_\phi(r) dr. \quad (2.3)$$

In this case, the converted photon spectrum is a line emission.

If dark matter is uniformly distributed in the universe, we would observe a continuum spectrum of the ALP intensity because free-streaming ALPs undergo a cosmological redshift

¹ESA, XMM-Newton, <http://sci.esa.int/xmm-newton>.

²Chandra X-ray observatory, <https://chandra.harvard.edu>.

in the expanding universe. Assuming light-mass ALPs, i.e. relativistic ALPs, produced by dark matter decay, a superposition of line spectra over different redshifts leads us to observe a continuum spectrum of ALPs [12, 13]:

$$\frac{dN}{dE_a} = \int_{\text{l.o.s.}} dr \frac{\Gamma_{\phi \rightarrow 2a}}{4\pi m_\phi} \rho_\phi(r) \times 2\delta_D(E_a(1+z) - m_\phi/2) \quad (2.4)$$

$$= \frac{\sqrt{2}c\Gamma_{\phi \rightarrow 2a}\rho_{\phi 0}}{\pi H_0} m_\phi^{-\frac{5}{2}} E_a^{\frac{1}{2}} f\left(\frac{m_\phi}{2E_a}\right) \quad (2.5)$$

where $\delta_D(x)$ is the Dirac delta function, and the function $f(x)$ is defined as

$$f(x) \equiv \left\{ \Omega_{m0} + (1 - \Omega_{m0} - \Omega_{\Lambda 0})/x - \Omega_{\Lambda 0}/x^3 \right\}^{-\frac{1}{2}}. \quad (2.6)$$

In the above equation z is the redshift at decay, $\rho_{\phi 0}$ is the present energy density, H_0 is present the Hubble constant, Ω_{m0} and $\Omega_{\Lambda 0}$ are the density parameters of non-relativistic matter and the cosmological constant, respectively. The spectral shape of ALPs is transcribed as a simple power-law function whose number index is a positive value of $+1/2$. In this case, the converted photon spectrum is also expected as a power-law function with a photon index of $+1/2$.

The ALP-photon conversion probability in a vacuum with a magnetic field via inverse Primakoff effect is given in ref. [14] as

$$P_{a \rightarrow \gamma}(x) = \left| \frac{g_{a\gamma\gamma}}{2} \int_0^x B_\perp(x') \exp\left(-i \frac{m_a^2}{2E_a} x'\right) dx' \right|^2, \quad (2.7)$$

with

$$B_\perp(x') \equiv \left| \vec{B}(x') \times \vec{e}_a \right|. \quad (2.8)$$

Here, $g_{a\gamma\gamma}$ is an ALP-photon coupling constant, m_a and E_a are mass and energy scales of ALP, and $B_\perp(x)$ is the perpendicular component of magnetic field to the ALP momentum direction, denoted as \vec{e}_a . The ALP-photon momentum transfer q is defined as

$$q = \frac{m_a^2}{2E_a}. \quad (2.9)$$

Assuming the $B_\perp(x')$ is uniform in the range $0 < x' < L$, we can write equation (2.7) as:

$$P_{a \rightarrow \gamma} = \left(\frac{g_{a\gamma\gamma} B_\perp}{2} \right)^2 2L^2 \frac{1 - \cos(qL)}{(qL)^2}. \quad (2.10)$$

In the limit of light ALP masses compared to the photon energy scale satisfying $qL \ll 1$, $1 - \cos(qL) \simeq (qL)^2/2$, and the conversion rate is simply given by

$$P_{a \rightarrow \gamma} = \left(\frac{g_{a\gamma\gamma} B_\perp L}{2} \right)^2. \quad (2.11)$$

under the coherence condition of

$$qL < \pi \rightarrow m_a < \sqrt{\frac{2\pi E_a}{L}} \quad (2.12)$$

The following analysis uses equation (2.10) to constrain the ALP-photon coupling constant.

As shown above, the probability of ALP particles converting to photons proportional to $(B_\perp L)^2$ in the light mass limit. Plugging typical values of the strength and coherent length scale of Earth's magnetic field, equation (2.11) gives

$$P_{a \rightarrow \gamma} \simeq 2.45 \times 10^{-21} \left(\frac{g_{a\gamma\gamma}}{10^{-10} \text{ GeV}^{-1}} \right)^2 \left(\frac{B_\perp L}{\text{T m}} \right)^2 \quad (2.13)$$

3 Analysis and results: a search for the correlation between residual *Suzaku* background radiation with the Earth’s magnetic strength

3.1 Selection of blank sky observations from *Suzaku* archival data

To locate ALP-induced photons, we use the *Suzaku* X-ray data, and search for photons in the detector’s field of view (FoV) depending on the integrated magnetic strength along the line-of-sight direction, $(B_{\perp}L)^2$. Because most X-ray data contains X-ray emission photons from targeted or unresolved sources, we need to study the X-ray diffuse background (XDB) in blank fields, and search for a residual signal in the background that is correlated with the magnetic strengths following the scaling of $(B_{\perp}L)^2$. The X-ray satellite *Suzaku* is suitable for this study because of its low instrumental background noise and the low background radiation from cosmic rays (compared to other X-ray satellites) due to its low-altitude Earth orbit; an altitude of ~ 570 km and an inclination of 31° from the Earth’s equatorial plane, where the Earth’s magnetic field prevents cosmic rays from penetrating the satellite’s detectors [6]. Figure 1 is a schematic illustration of the *Suzaku* orbit and the Earth’s magnetic field configuration. Even if the satellite observes the same field or the same angular direction — as denoted by the black dotted line — the integrated strength of perpendicular magnetic components along the line-of-sight direction varies with the satellite position. The *Suzaku* satellite orbits the Earth with a period of approximately 96 minutes and it causes a modulation of the integrated magnetic strength $(B_{\perp}L)^2$ with the orbit, or when the target field is observed. Thus, we expect variations in the ALP-induced photons, if they exist, depending on the strength $(B_{\perp}L)^2$. We calculated the Earth’s magnetic field every 60 seconds for each line-of-sight direction of a given target field using the software, *International Geomagnetic Reference Field*: the 12th generation (IGRF-12 [15]) for up to 6 times the Earth’s radius (R_E), where typically $B \sim 10^{-7}$ T. The right panel in figure 1 shows a typical case of $(B_{\perp}L)^2$ as a function of the satellite position or equivalently the observation time. It can be found that a typical value of $(B_{\perp}L)^2$ is of order of 10^4 – 10^5 T²m², which is greater than that of terrestrial experiments such as the CAST experiment.³ If we apply the non-oscillation condition of $qL \ll 1$ (equation (2.12)), the corresponding mass of ALP is limited to be $m_a \leq \mu\text{eV}$ if we assume that the converted photons are in X-ray wavelengths. Note that we considered an oscillation regime of $qL \sim 1$ to obtain constraints on the ALP-photon coupling constant.

To estimate the XDB spectrum, we consider blank sky data from four deep fields selected from the *Suzaku* archives as tabulated in table 1. The selection criteria are as follows.

1. No bright sources in the FoV of *Suzaku* X-ray Imaging Spectrometer (XIS) [16], and compact sources in the FoV are already identified and can be masked in our analysis.
2. Galactic latitudes of $|b| > 20^\circ$ to avoid X-ray emission originating from sources in the Galactic disk [17].
3. Sufficiently distant from regions of high X-ray diffuse emissions such as the North Polar Spur.
4. Exposure time obtained by standard processing should be more than 200 ksec.

The above criteria are met by the following four fields, also shown in table 1. First, we use the multiple observation data in the Lockman hole field, which is a famous region with minimum

³CERN axion solar telescope, <http://cast.web.cern.ch/CAST/CAST.php>.

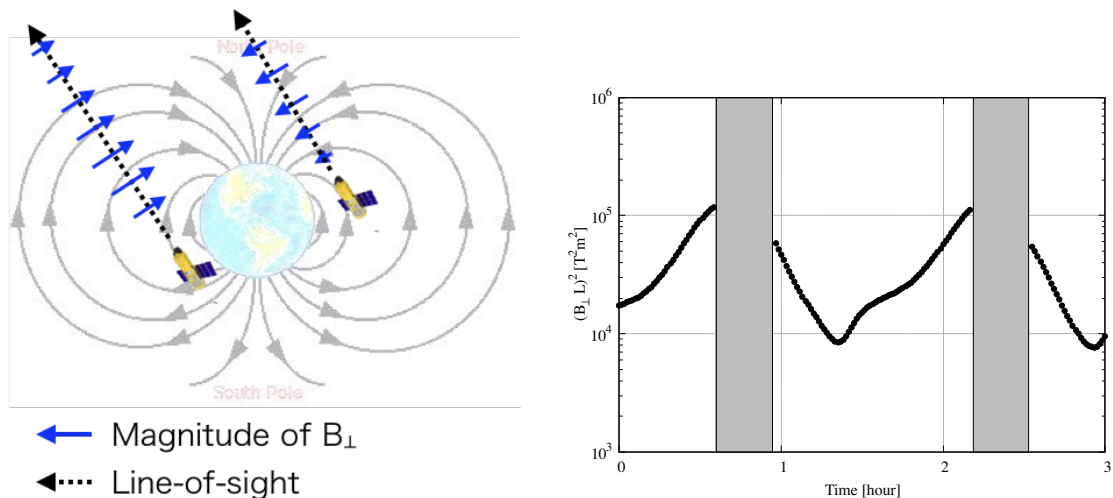


Figure 1. Left: schematic view of the position and observation direction of *Suzaku* satellite relative to the Earth’s magnetosphere. Right: time dependence of $(B_{\perp}L)^2$ in a Lockman hole observation. Gray hatched regions show periods of the Earth occultation, i.e. the Earth exists between a target and *Suzaku*.

Field name	$(\alpha_{2000}, \delta_{2000})$	Num. of Obs.	Total exposure* [ksec]	Num. of events [†] [counts]	Exposure used in this analysis [†] [ksec]	Obs. Year
Lockman hole	(162.9, 57.3)	11	542.5	5595	210.7	2006–2014
MBM16	(49.8, 11.7)	6	446.9	10755	231.8	2012–2015
NEP	(279.1, 66.6)	4	205.0	7666	221.9	2009
SEP	(90.0, -66.6)	4	204.2	6102	180.2	2009

* Exposure time at each XIS after the standard data processing pipeline.

[†] The sum of the three XIS exposure time after extra data reduction and $(B_{\perp}L)^2$ selection, used values in this paper.

Table 1. Observation of long exposure background observation by *Suzaku* satellite.

neutral hydrogen column density that was annually observed with *Suzaku* for calibration. We also use the data in the South Ecliptic Pole (SEP) and North Ecliptic Pole (NEP) fields. Finally, we use the data in the field of high latitude, the neutral hydrogen cloud or the so-called MBM16 field.

We use the data reduction pipelines, the *Ftools* in HEASoft version 6.16 and XSPEC version 12.8.2, to analyze the X-ray data in the four fields of table 1, collected from the archive of *Suzaku* XIS. To avoid a possible contamination from high X-ray background, we removed data during the South Atlantic Anomaly region, Earth occultation, low elevation angle from the Earth’s rim, and low cut-off-rigidity (COR; ≤ 8 GV/c) regions. We stacked the X-ray image in the 0.5–7 keV band for each of the four fields, where we removed the point sources whose flux is larger than 1×10^{-14} ergs s^{−1} cm^{−2}, with a radius of 1.5 arcminutes corresponding to encircled power function of 90% for *Suzaku*’s mirror. We then calculated

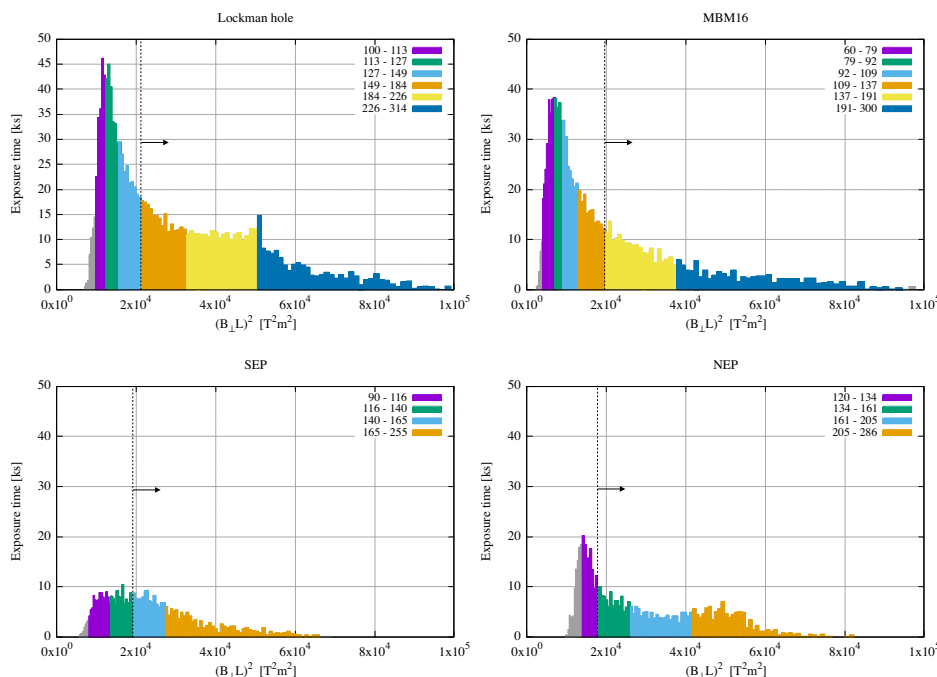


Figure 2. The histograms of $(B_{\perp}L)^2$ during observation of 4 direction. Binning of exposure time, to obtain an almost equal number of photons in each class of $(B_{\perp}L)^2$ are shown. Note that only $(B_{\perp}L)^2 \geq 2 \times 10^4 \text{ T}^2 \text{ m}^2$ are used for spectral analysis as shown in section 3.2.

the $(B_{\perp}L)^2$ every 60 seconds for each observation, as a function of the satellite position in orbit and observing line-of-sight direction. Figure 2 shows the distribution of $(B_{\perp}L)^2$ in each of the four fields. We subdivided the data into four to six bins of the $(B_{\perp}L)^2$ values, where the binning was determined so that each bin had almost the same photon statistics, as denoted by the different colored histograms in the figure.

3.2 An assessment of non-Xray background contamination

Before presenting the main results, we need to assess the level of non-Xray background (NXB) contamination in the data. Although the NXB of *Suzaku* is usually low, there could be a residual NXB contamination, up to 16–50% of the observed CXB in the 2–6 keV range. A part of NXB is due to fluorescence lines by materials such as Si, Al, Au, and Ni around the detector. These lines are distinguishable, if their emission lines are identified at their corresponding energy scales, in each XIS spectrum, as identified in ref. [18]. Not only X-rays but charged particles too can produce pseudo-events in the CCD instrument. Pseudo events produced by particles originating from cosmic rays in orbit were studied by GEANT4 Monte-Carlo simulation. The continuum spectra by pseudo events are reproducible at an accuracy of 20% in its amplitude in each energy bin [19]. The production processes of pseudo events are well understood, but the input cosmic-ray flux varies by time and position of the satellite. The reproduction of the events was studied by using the event database collected during the periods when the FoV was blocked by the night side of the Earth (NTE) [20]. It was found that the intensity of the background could be estimated as a function of COR, and that the spectra were similar. They proposed a background estimation method to make a spectrum

from ± 150 days of stacked night-Earth data weighted to reproduce the distribution of COR. They also found that the fluctuation of the background is larger than the simple Poisson statistics. Uncertainty of reproducibility for a typical 50 ksec exposure was reported to be 3.4%, although the expected statistical error by Poisson statistics is 1/10 [20]. This procedure is used as a standard background estimation for *Suzaku* and adapted as a HEASoft tool.

In our analysis, we needed to sort the data by $(B_{\perp}L)^2$, which correlated with the COR. If the orbital position or $(B_{\perp}L)^2$ is a potential control parameter of the NXB, it will affect our determination of the $(B_{\perp}L)^2$ modulated signal. COR parameters used in the *Suzaku* analysis (defined as COR2 in the calibration database) are defined by the projected geographic coordinates, and calculated by the geomagnetic model on 2006 Apr. Actual COR would change gradually with time, and the cosmic ray flux is affected by the solar activity. We thus stepped into further NXB analysis of *Suzaku*, to evaluate possible range of background fluctuation, and to define further data reduction methods if needed.

We evaluated the fluctuation of input cosmic-ray flux by event rates at 12–15 keV of the XIS1. As the effective area of the X-ray mirror dropped rapidly above the Au L-edge below 1%, the event rate above 12 keV is considered to be an indicator of the cosmic ray flux. Due to the back-illumination structure, the background rate of XIS1 is higher than the other front-illuminated CCD, XIS0 and XIS3, and is more sensitive. Apparently, the fluctuation of the background count rate exceeds the Poisson statistics. In [20], the intrinsic fluctuation is evaluated as $\sqrt{\sigma_{\text{calc}}^2 - \sigma_{\text{Poisson}}^2}$. We evaluate the intrinsic fluctuation as follows:

1. Counting the number of events in 12–15 keV during the 60 sec for each COR range.
2. Calculating an mean of the count every 60 sec bins, denoted as μ , from the distribution of count rate as shown in histogram in figure 3.
3. Assuming a certain value σ , and simulating a P_{NXB} by Monte-Carlo method as shown in equation (3.1) (lines in figure 3).

$$P_{\text{NXB}}(X = k) = \frac{\lambda(k, \sigma)^k e^{-\lambda(k, \sigma)}}{k!}, \quad \lambda(k, \sigma) = \frac{1}{\sqrt{2\pi}\sigma^2} \exp\left(-\frac{(k - \mu)^2}{2\sigma^2}\right), \quad (3.1)$$

where k is an observation frequency per interval, $\lambda(k, \sigma)$ is an average number of events per interval, σ is an estimated systematic error by the variation of $\lambda(k, \sigma)$, and μ is an average of observed NXB events.

4. Comparing the observed and simulated histograms by Pearson's chi-squared test and obtaining 95% upper limit for σ .

It assumes that the variations of the mean value of the count rates follow a Gaussian distribution, and the detected count follows a Poisson distribution. Thus, the observed count rate is expressed by a convolution of these functions. We use Pearson's chi-squared test to set a quantitative upper limit for the short term variability. A sample of these tests is shown in figure 3. The 95% confidence range for the standard deviation of the Gaussian is obtained as 22–39% of the mean value.

The background rate anomaly of the geographical position is checked as follows. We divided the orbital position projected onto the Earth's surface by every 10° in longitude and 5° in latitude as defined as Loc_ID, and sorted them into 4 COR classes. For each observation, the NTE count rate in 2–5.6 keV for ± 150 days, which is used by the standard background

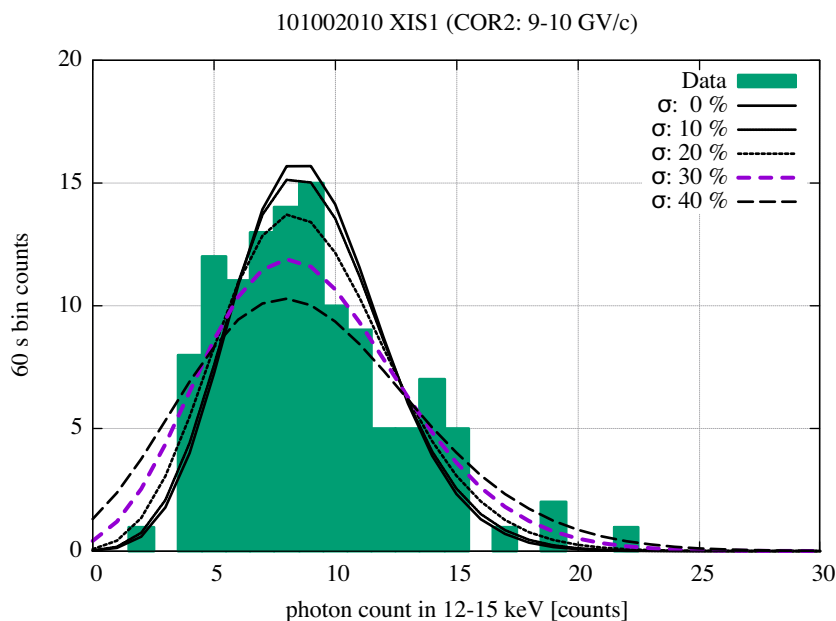


Figure 3. A sample of histogram for observed events in 12–15 keV of XIS1 in COR range of 9 to 10 GV/ c and the probability distribution of each σ/μ estimated from equation (3.1).

estimation, was accumulated on every `Loc_ID`. If the count rate at an `Loc_ID` is higher than the averaged value over the same COR class by 3σ , the events occurred at that `Loc_ID` were discarded from the spectral analysis.

After these data were reduced, the count rate in 2–6 keV before and after the standard background subtraction were plotted as a function of $(B_{\perp}L)^2$. We found that there is a negative correlation between the count rate and the $(B_{\perp}L)^2$, contrary to the ALP origin signal prediction. We checked the count rate of the upper discriminator (PIN-UD) of the Hard X-ray Detector (HXD) onboard *Suzaku*, which corresponds to energy deposited by protons approximately > 100 MeV [21], and found the same trend. The PIN-UD is affected by the radio-activation of HXD itself, and cannot be used to estimate the XIS background. We evaluated the correlation by a linear function fit, and decided that only those data satisfying $(B_{\perp}L)^2 \geq 2 \times 10^4 \text{ T}^2 \text{ m}^2$ would be used for the analysis.

3.3 Spectral analysis for $(B_{\perp}L)^2$ sorted data

In the spectral analysis, we assumed that celestial diffuse emission of each blank field is expressed by the sum of Cosmic X-ray Background (CXB), Milky Way Halo (MWH) emission, Solar Wind Charge eXchange (SWCX), Local Hot Bubble (LHB), and unknown High Temperature Component (HTC) as studied by previous works [11, 22, 23]. These are collectively called XDB. The surface brightness and spectral parameters for the celestial emission can be varied by the FoV in a reasonable range. The ALP signal has a power-law spectral shape with a photon index of $+1/2$, and with intensities proportional to $(B_{\perp}L)^2$. The NXB for each observation can be estimated by the standard background estimation method [20], but the intensities can also be varied within the fluctuation studied in the previous subsection.

Steps of spectral analysis for one observing direction are as follows;

0. Apply standard data reduction for XIS 0,1,3 of each observation ID (a unit of archival data, events from continuous pointing for the same observation direction), point source

removal, `Loc_ID` selection and $(B_{\perp}L)^2$ cut. Response matrices [24] and template NXB by standard method [20] are also prepared.

1. Accumulate the energy spectra in the 0.7–7.0 keV range for each XIS 0,3 and the 0.7–5.0 keV range for XIS 1 subtract the standard NXB, and fit them simultaneously by an empirical X-ray background model, obtained the best-fit values and errors with χ^2 statistics and C -statistics [25] in *Xspec*, and evaluate the validity of parameters.
2. Divide the energy spectra by $(B_{\perp}L)^2$ values and fit them again simultaneously with C -statistics because of low photon statistics in each range. Check the consistency of spectral parameters obtained in step 1.
3. Add ALP emission model as a power-law function with a photon index of +1/2 and with a surface brightness proportional to the $(B_{\perp}L)^2$, and treat the background as a spectral model whose intensities can be tuned.

The fitting model describing the diffuse X-ray emission is similar to that used in [11]; it is shown by

$$apec_{\text{SWCX+LHB}} + phabs(apec_{\text{MWH}} + power-law_{\text{CXB}} + apec_{\text{HTC}}).$$

The APEC (Astrophysical Plasma Emission Code) [26]⁴ is an emission model from collisional equilibrium and optically thin plasma installed in *Xspec* and applied to estimate the SWCX and LHB blend, MWH, and HTC. The temperature of *apec* in the SWCX and LHB blend was fixed to $kT = 0.1$ keV [27]. The typical temperature of the MWH is $kT = 0.15$ – 0.35 keV [11, 22], a part of the blank sky spectra requires a HTC with $kT = 0.6$ – 0.9 keV to describe emission of approximately 0.9 keV [11]. The CXB was represented by a power-law emission model with a photon index of ~ 1.4 . The solar abundance table of *apec* model was given by [28]. *Phabs* describes the absorption by the Galactic interstellar medium, whose column density is fixed from the LAB(Leiden/Argentine/Bonn) survey [29] database. Steps 0–1 are the standard spectral fitting procedure for *Suzaku*, and the parameters obtained in step 1 were consistent with each other within 90% error, and with previous works like Sekiya et al. (2016) [11].

In step 2, we divided the data by $(B_{\perp}L)^2$. For example, in the case of Lockman hole, there were 11 observations, sorted by $(B_{\perp}L)^2$ into 3 classes, and 3 CCDs, thus 99 spectra were fitted simultaneously with the same emission parameter. The number of the energy spectra for Lockman hole, MBM 16, SEP, and NEP, are 99, 36, 24, and 36, respectively. The degrees of freedom in the spectral fit also increased, and the number of photons in each energy bin decreased. We applied C -statistics, which assumes that the data follows a Poisson distribution and uses the likelihood ratio to be minimized, and confirmed that the obtained parameters are consistent with step 1. Because we would divide the spectra in later analysis, complex structure (mainly of Oxygen lines below 0.7 keV) are not well resolved. We only used the data in from the 0.7–7.0 keV range. Some components whose intensities were consistent with null were ignored by setting the intensities to 0.

In step 3, we added the ALP component whose surface brightness is proportional to $(B_{\perp}L)^2$. In usual spectral fitting like steps 1–2, we used the spectra after subtraction of the estimated background. Here, we treated the NXB as one of the input models with a normalization factor, which can be variable in each observation ID, CCD, and $(B_{\perp}L)^2$

⁴Latest version is available at <http://www.atomdb.org>.

Model	Parameter	Lockman hole	MBM16	SEP	NEP
Num of Obs.ID		11	6	4	4
Num of $(B_{\perp}L)^2$ classification*		3	2	2	3
Absorption	N_{H} [10^{20} cm^{-2}]	0.58(fix)	16.90(fix)	4.72(fix)	3.92(fix)
LHB+SWCX	kT [keV]	-	-	0.1(fix)	-
	Norm [†]	0(fix)	0(fix)	$33.4^{+88.9}_{-33.4}$	0(fix)
MWH	kT_1 [keV]	$0.14^{+0.08}_{-0.09}$	$0.32^{+0.24}_{-0.23}$	-	$0.21^{+0.18}_{-0.13}$
	Norm [†] ₁	28^{+622}_{-20}	$2.1^{+23.0}_{-1.3}$	0(fix)	$4.1^{+13.5}_{-3.9}$
HTC	kT_2 [keV]	0.61^{\P}	-	$0.66^{+0.08}_{-0.06}$	0.69
	Norm [†] ₂	$0.5^{+0.4}_{-0.5}$	0(fix)	$2.1^{+0.5}_{-0.6}$	$0.3^{+0.7}_{-0.3}$
CXB	Γ_{CXB}	$-1.42^{+0.13}_{-0.13}$	$-1.33^{+0.16}_{-0.16}$	$-1.50^{+0.23}_{-0.25}$	$-1.53^{+0.18}_{-0.18}$
	$S_{\text{CXB}}^{\ddagger}$	$7.7^{+0.6}_{-0.6}$	$6.5^{+1.1}_{-1.0}$	$5.6^{+0.9}_{-0.8}$	$6.9^{+0.7}_{-0.8}$
ALP	Γ_{ALP}	+0.5(fix)	+0.5(fix)	+0.5(fix)	+0.5(fix)
	S_{ALP}^{\S}	$0.012^{+0.015}_{-0.016}$	$0.005^{+0.022}_{-0.024}$	$0.011^{+0.027}_{-0.030}$	$0.012^{+0.020}_{-0.022}$
$C/\text{dof}(\text{dof})$		1.11(2865)	1.03(1505)	0.99(1000)	1.10(1503)

All errors indicate 90% confidence level.

* See classification shown in figure 2.

[†] The emission measure of CIE plasma integrated over the line-of-sight for SWCX+LHB, MWH (the normalization of *apec* model): $(1/4\pi) \int n_e n_H ds$ in unit of $10^{14} \text{ cm}^{-5} \text{ sr}^{-1}$.

[‡] The surface brightness of the CXB (the normalization of a power-law model): in unit of photons $\text{cm}^{-2} \text{ sec}^{-1} \text{ keV}^{-1} \text{ str}^{-1}$ at 1 keV.

[§] The surface brightness of the ALP (the normalization of a power-law model): in unit of photons $\text{cm}^{-2} \text{ sec}^{-1} \text{ keV}^{-1} \text{ str}^{-1}$ at 1 keV and $10^4 \text{ T}^2 \text{ m}^2$.

^{\P} Parameter pegged at fitting limit: 0.

^{\|} Because the normalization of *apec* allows 0 within the error range, the temperature is not determined.

Table 2. Summary of best-fit parameters of the XDB + ALP + NXB model by spectral fitting in Lockman Hole, MBM16, SEP, and NEP observation with $(B_{\perp}L)^2$ sorted.

class. In contrast, the parameters for celestial emission and the normalization of the ALP component at a fixed $(B_{\perp}L)^2 = 10^4 \text{ T}^2 \text{ m}^2$ are common for the same FoV. The final fitting results are summarized in table 2. We assumed the flux of the ALP both in negative and positive mathematically to evaluate proper error ranges, as shown in figure 4.

In all four observational directions, the surface brightness for the ALP components is consistent with 0 within a 90% confidence level. We also checked that the normalizations of the NXB model were within $\pm 40\%$, or the fluctuation studied in section 3.2. We made contour plots by surface brightness of ALP and CXB components between 2–6 keV, as shown in figure 4. As the surface brightness varies with the index and normalization of an assumed power-law part, the contour is not smooth, owing to the steps in the parameter search. The limit obtained from the MBM16 observation is the lowest among these four fields and gives the tightest upper limit on the ALP flux: $1.6 \times 10^{-9} \text{ ergs s}^{-1} \text{ cm}^{-2} \text{ sr}^{-1}$ normalized at $10^4 \text{ T}^2 \text{ m}^2$. An accumulated spectrum of all fitted data is shown in figure 6 with averaged XDB and NXB model and the obtained upper limit for ALP. In table 3, we also tabulated the center values of the CXB surface brightness and the upper limits of the ratio of ALP emission hidden in the CXB.

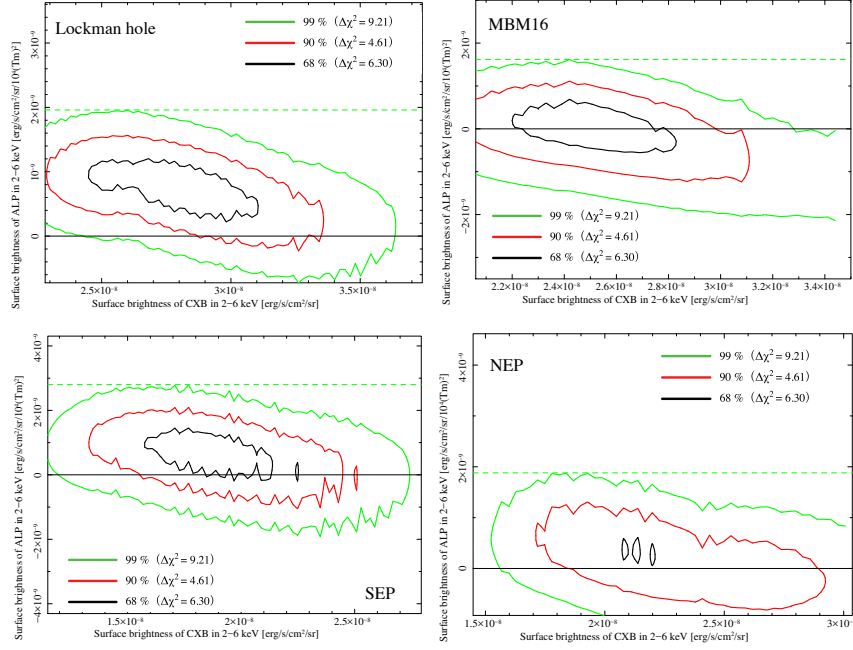


Figure 4. The confidence contour between surface brightness of CXB and ALP calculated from the photon index Γ_{CXB} , Γ_{ALP} and normalization S_{CXB} , S_{ALP} as shown in table 2 obtained for Lockman hole, MBM16, SEP, and NEP observations, where the NXB normalization parameters were allowed to vary. 3 confidence levels: 68% (black), 90% (red) and 99% (green). Dashed line: 99% upper limit for ALP surface brightness.

Field Name	99% UL for ALP surface brightness*	best-fit CXB surface brightness [†]	99% UL for CXB ratio [%]
Lockman hole	2.0	28.3	7.1
MBM16	1.6	26.9	5.9
SEP	2.8	18.6	15.1
NEP	1.9	22.0	8.6

* In unit of $10^{-9} \text{ ergs s}^{-1} \text{ cm}^{-2} \text{ sr}^{-1}$ at $10^4 \text{ T}^2 \text{ m}^2$ in 2–6 keV band.

[†] In unit of $10^{-9} \text{ ergs s}^{-1} \text{ cm}^{-2} \text{ sr}^{-1}$ in 2–6 keV band.

Table 3. Summary of upper limit at 99% confidence level of surface brightness for ALP origin emissions as shown by dashed line in figure 4.

To show the degeneracy among ALP and NXB normalization, we made a contour plot with the Lockman hole observation at one Obs. ID, one BL class, and one XIS, as shown in figure 5. In the case of the Lockman hole, we have independently determined NXB normalization for all 11Obs. ID, 3 BL classes, and 3 XISs.

4 Discussion and conclusions

We assumed that the cosmologically distributed ALPs would make a power-law with a photon index of +0.5 ($dN/dE \propto E^{+0.5}$) emission by the Earth’s magnetosphere in proportion to

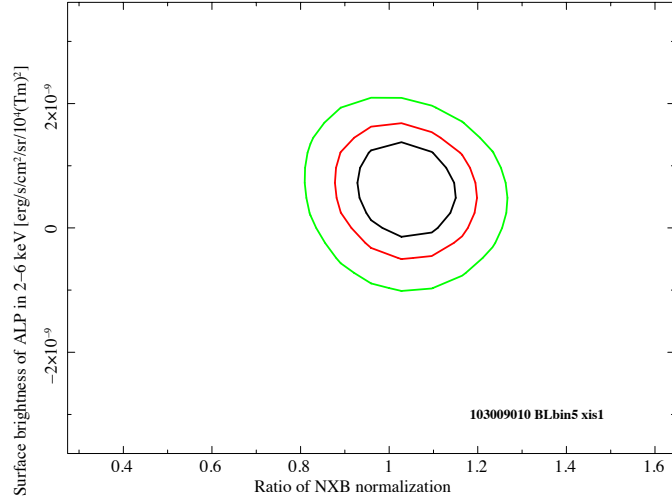


Figure 5. The confidence contour between ratio of NXB normalization and surface brightness of ALP calculated from the photon index Γ_{ALP} and normalization S_{ALP} as shown in table 2 obtained for Lockman hole at one Obs. ID, one $(B_{\perp}L)^2$ class, and one XIS. 3 confidence levels: 68% (black), 90% (red) and 99% (green).

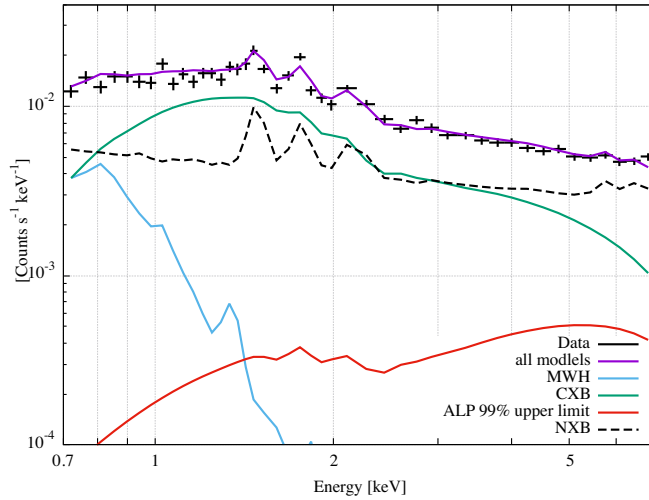


Figure 6. Accumulated spectrum used in the spectral fit for MBM16 direction. The spectrum is the sum of all Obs.ID, $(B_{\perp}L)^2$ classes, and XISs. A response is weighted by the number of photons, and the NXB model is weighted by the exposure time after applying the normalization constant. Note that actual fitting was done with a set of energy spectra simultaneously, and no residuals are shown.

the integrated $(B_{\perp}L)^2$ in the FoV, and analyzed the data with *Suzaku* for four different directions. We did not detect any possible continuous emission from ALPs reported by previous similar studies [7]. We obtained the 99% upper limit of the X-ray surface brightness and flux originating from ALPs in the 2.0–6.0 keV energy range as $1.6 \times 10^{-9} \text{ ergs s}^{-1} \text{ cm}^{-2}$

sr^{-1} , at $(B_{\perp}L)^2 = 10^4 \text{ T}^2 \text{ m}^2$, as shown in table 3. It corresponds to 6–15% of the apparent CXB surface brightness in the 2–6 keV band, and is consistent with the idea that 80–90% of the CXB in the 2–8 keV band are resolved into point sources [30, 31]. In other words, it could not be denied that 10–20% of the unresolved CXB could originate from the ALP converted to X-ray by the Earth atmosphere at *Suzaku* orbit.

If we assume the dark matter density and decay rate, we can limit the ALP-photon coupling constant. By combining equations (2.5), (2.6) and (2.13), the ALP-photon coupling constant, $g_{a\gamma\gamma}$, was constrained in the ALP mass range of $m_a < \sqrt{2\pi E_a/L} \sim 3.3 \times 10^{-6} \text{ eV}$ to be

$$g_{a\gamma\gamma} < 3.3 \times 10^{-7} \text{ GeV}^{-1} \left(\frac{m_{\phi}}{10 \text{ keV}} \right)^{5/4} \left(\frac{\tau_{\phi}}{4.32 \times 10^{17} \text{ s}} \right)^{1/2} \left(\frac{B_{\perp}L}{100 \text{ T m}} \right)^{-1} \\ \left(\frac{\rho_{\phi}}{1.25 \text{ keV cm}^{-3}} \right)^{-1/2} \left(\frac{H_0}{67.8 \text{ km s}^{-1} \text{ Mpc}^{-1}} \right)^{-1/2} \left(\frac{f}{1.92} \right)^{-1/2}, \quad (4.1)$$

as shown in figure 7. Here, we assume a standard cosmology model with a mass density and a Hubble constant H_0 . The decay rate of the dark matter to the ALPs $\Gamma_{\phi \rightarrow 2a} = 1/\tau_{\phi} < 1/t_0$, where t_0 is the Hubble time. The factor f is defined by the equation (2.6). Note that we neglect the reduction and anisotropy of the ALP flux due to interstellar and intergalactic magnetic fields.

For the line emission search in the X-ray band, Sekiya et al. (2016) collected the longest exposure of 12 Msec from 10 years of *Suzaku* archival data, and obtained a 3σ upper limit for a narrow line emission between 1 and 7 keV to be $0.021 \text{ photons s}^{-1} \text{ cm}^{-2} \text{ sr}^{-1}$ [11]. The ALP-photon conversion rate, $P_{a \rightarrow \gamma} \propto (B_{\perp}L)^2$, was also computed by using IGRF-12 model every 60 seconds, and the averaged value was obtained to be $(B_{\perp}L) = 140 \text{ T m}$. It is larger than the value of 84 T m by CAST [32]. This value gives the upper limits of

$$I_{a,\text{line}} \cdot \left(\frac{g_{a\gamma\gamma}}{10^{-10} \text{ GeV}^{-1}} \right)^2 < 4.4 \times 10^{14} \text{ axions s}^{-1} \text{ cm}^{-2} \text{ sr}^{-1} \quad \text{in the 1.0–7.0 keV band.} \quad (4.2)$$

A $g_{a\gamma\gamma}$ can be also constrained as

$$g_{a\gamma\gamma} < 8.4 \times 10^{-8} \text{ GeV}^{-1} \left(\frac{B_{\perp}L}{140 \text{ T m}} \right)^{-1} \left(\frac{\tau_{\phi}}{4.32 \times 10^{17} \text{ s}} \right)^{1/2} \left(\frac{S_{\phi}}{50 \text{ M}_{\odot} \text{ pc}^{-2}} \right)^{-1/2}, \quad (4.3)$$

when the ALP density is connected with dark matter density around our galaxy. It is also shown in figure 7 as galactic monochromatic ALP. In the plot, we consider the oscillation effect by equation (2.10). This restriction of a physical parameter of ALPs is less strict than other experiments (e.g. CAST, ADMX), which assume a different axion and ALP model than this research. Nevertheless, it is important to note that we found these restrictions by using a new independent method from X-ray observations.

Acknowledgments

This work was partially supported by JSPS KAKENHI Grant Numbers 26220703 and 14J11023. We thank Prof. M. Kawasaki and Prof. M. Teshima for valuable comments, and Dr. N. Sekiya for using his data and suggestions. We would like to thank Editage (www.editage.com) for English language editing.

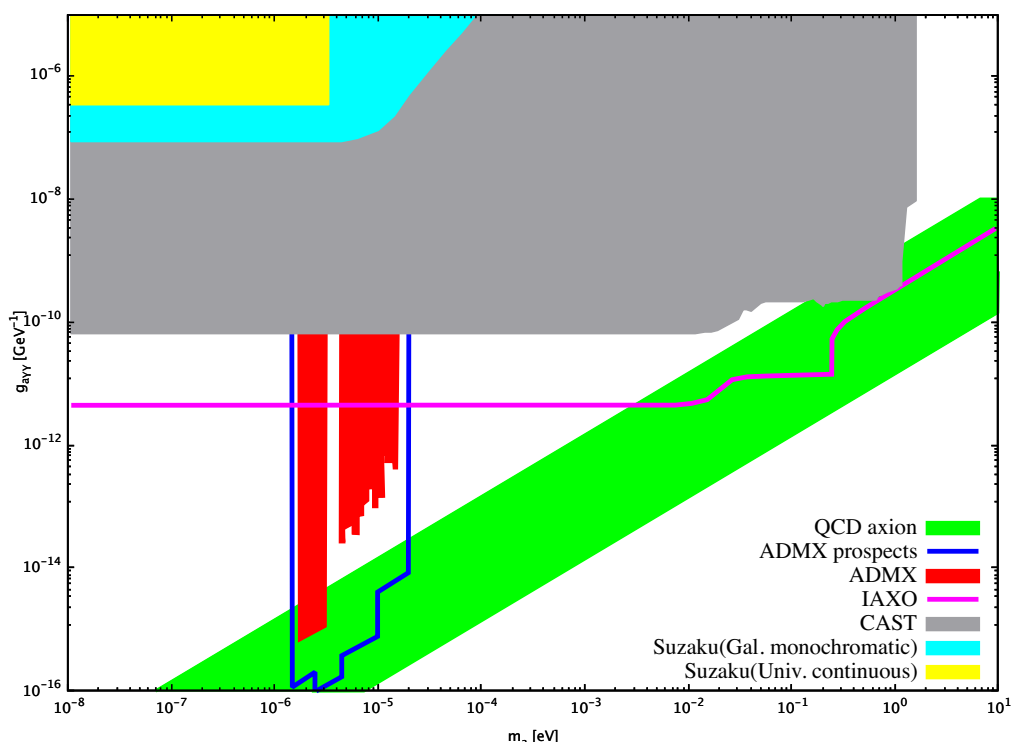


Figure 7. ALP parameters constraints in this paper in Universal continuous ALP (cyan) and Galactic monochromatic ALP (yellow) see details in text. Limits of other experiments are taken from [33, 34]

References

- [1] R.D. Peccei and H.R. Quinn, *CP conservation in the presence of instantons*, *Phys. Rev. Lett.* **38** (1977) 1440 [[INSPIRE](#)].
- [2] S. Weinberg, *A new light boson?*, *Phys. Rev. Lett.* **40** (1978) 223 [[INSPIRE](#)].
- [3] M. Cicoli, J.P. Conlon, M.C.D. Marsh and M. Rummel, *3.55 keV photon line and its morphology from a 3.55 keV axionlike particle line*, *Phys. Rev. D* **90** (2014) 023540 [[arXiv:1403.2370](#)] [[INSPIRE](#)].
- [4] J.P. Conlon and F.V. Day, *3.55 keV photon lines from axion to photon conversion in the Milky Way and M31*, *JCAP* **11** (2014) 033 [[arXiv:1404.7741](#)] [[INSPIRE](#)].
- [5] J.P. Conlon and A.J. Powell, *A 3.55 keV line from $DM \rightarrow a \rightarrow \gamma$: predictions for cool-core and non-cool-core clusters*, *JCAP* **01** (2015) 019 [[arXiv:1406.5518](#)] [[INSPIRE](#)].
- [6] K. Mitsuda et al., *The X-ray observatory Suzaku*, *Publ. Astron. Soc. JPN* **59** (2007) S1.
- [7] G.W. Fraser, A.M. Read, S. Sembay, J.A. Carter and E. Schyns, *Potential solar axion signatures in X-ray observations with the XMM-Newton observatory*, *Mon. Not. Roy. Astron. Soc.* **445** (2014) 2146 [[arXiv:1403.2436](#)] [[INSPIRE](#)].
- [8] H. Davoudiasl and P. Huber, *Detecting solar axions using earth's magnetic field*, *Phys. Rev. Lett.* **97** (2006) 141302 [[hep-ph/0509293](#)] [[INSPIRE](#)].
- [9] H. Davoudiasl and P. Huber, *Feasibility study for measuring geomagnetic conversion of solar axions to X-rays in low earth orbits*, *JCAP* **08** (2008) 026 [[arXiv:0804.3543](#)] [[INSPIRE](#)].

- [10] M. Roncadelli and F. Tavecchio, *No axions from the Sun*, *Mon. Not. Roy. Astron. Soc. Lett.* **450** (2015) L26.
- [11] N. Sekiya, N.Y. Yamasaki and K. Mitsuda, *A search for a keV signature of radiatively decaying dark matter with Suzaku XIS observations of the X-ray diffuse background*, *Publ. Astron. Soc. JPN* **68** (2016) S31.
- [12] M. Kawasaki and T. Yanagida, *Constraint on cosmic density of the string moduli field in gauge mediated supersymmetry breaking theories*, *Phys. Lett. B* **399** (1997) 45 [[hep-ph/9701346](#)] [[INSPIRE](#)].
- [13] T. Asaka, J. Hashiba, M. Kawasaki and T. Yanagida, *Spectrum of background x-rays from moduli dark matter*, *Phys. Rev. D* **58** (1998) 023507 [[hep-ph/9802271](#)] [[INSPIRE](#)].
- [14] K. van Bibber, P.M. McIntyre, D.E. Morris and G.G. Raffelt, *A practical laboratory detector for solar axions*, *Phys. Rev. D* **39** (1989) 2089 [[INSPIRE](#)].
- [15] E. Thébault et al., *International geomagnetic reference field: the 12th generation*, *Earth Planets Space* **67** (2015) 79.
- [16] K. Koyama et al., *X-ray imaging spectrometer (XIS) on board Suzaku*, *Publ. Astron. Soc. Jpn* **59** (2007) S23.
- [17] K. Masui et al., *The nature of unresolved soft X-ray emission from the galactic disk*, *Publ. Astron. Soc. Jpn* **61** (2009) S115.
- [18] H. Yamaguchi et al., *The background properties of Suzaku/XIS*, *Proc. SPIE* **6266** (2006) 626642.
- [19] H. Murakami, M. Kitsunezuka, M. Ozaki, T. Dotani and T. Anada, *Origins of the instrumental background of the x-ray CCD camera in space studied with Monte Carlo simulation*, *Proc. SPIE* **6266** (2006) 62662Y.
- [20] N. Tawa et al., *Reproducibility of non-X-ray background for the X-ray imaging spectrometer aboard Suzaku*, *Publ. Astron. Soc. Jpn* **60** (2008) S11.
- [21] M. Kokubun et al., *In-orbit performance of the hard X-ray detector on board Suzaku*, *Publ. Astron. Soc. Jpn* **59** (2007) S53.
- [22] T. Yoshino et al., *Energy Spectra of the Soft X-Ray Diffuse Emission in Fourteen Fields Observed with Suzaku*, *Publ. Astron. Soc. Jpn* **61** (2009) 805.
- [23] S. Nakashima, Y. Inoue, N. Yamasaki, Y. Sofue, J. Kataoka and K. Sakai, *Spatial distribution of the milky way hot gaseous halo constrained by Suzaku X-ray observations*, *Astrophys. J.* **862** (2018) 34.
- [24] Y. Ishisaki et al., *Monte Carlo simulator and ancillary response generator of Suzaku XRT/XIS system for spatially extended source analysis*, *Publ. Astron. Soc. Jpn* **59** (2007) S113.
- [25] W. Cash, *Parameter estimation in astronomy through application of the likelihood ratio*, *Astrophys. J.* **228** (1979) 939 [[INSPIRE](#)].
- [26] R.K. Smith, N.S. Brickhouse, D.A. Liedahl and J.C. Raymond, *Collisional plasma models with APEC/APED: emission line diagnostics of hydrogen-like and helium-like ions*, *Astrophys. J.* **556** (2001) L91 [[astro-ph/0106478](#)] [[INSPIRE](#)].
- [27] H. Yoshitake, K. Sakai, K. Mitsuda, N. Y. Yamasaki, Y. Takei and R. Yamamoto, *Long-term variability of the O VII line intensity toward the Lockman hole observed with Suzaku from 2006 to 2011*, *Publ. Astron. Soc. Jpn* **65** (2013) 32.
- [28] E. Anders and N. Grevesse, *Abundances of the elements: meteoritic and solar*, *Geochim. Cosmochim. Acta* **53** (1989) 197 [[INSPIRE](#)].

- [29] P.M.W. Kalberla et al., *The Leiden/Argentine/Bonn (LAB) survey of Galactic HI: final data release of the combined LDS and IAR surveys with improved stray-radiation corrections*, *Astron. Astrophys.* **440** (2005) 775 [[astro-ph/0504140](#)] [[INSPIRE](#)].
- [30] N. Cappelluti et al., *The Chandra COSMOS legacy survey: energy spectrum of the cosmic X-ray background and constraints on undetected populations*, *Astrophys. J.* **837** (2017) 19 [[arXiv:1702.01660](#)] [[INSPIRE](#)].
- [31] B. Luo et al., *The Chandra deep field-south survey: 7 Ms source catalogs*, *Astrophys. J. Suppl.* **228** (2017) 2 [[arXiv:1611.03501](#)] [[INSPIRE](#)].
- [32] CAST collaboration, *An improved limit on the axion-photon coupling from the CAST experiment*, *JCAP* **04** (2007) 010 [[hep-ex/0702006](#)] [[INSPIRE](#)].
- [33] G. Carosi, A. Friedland, M. Giannotti, M.J. Pivovarov, J. Ruz and J.K. Vogel, *Probing the axion-photon coupling: phenomenological and experimental perspectives. A snowmass white paper*, in *Proceedings, 2013 Community Summer Study on the Future of U.S. Particle Physics: Snowmass on the Mississippi (CSS2013): Minneapolis, MN, U.S.A., 29 July-6 August 2013*, (2013), [arXiv:1309.7035](#), <http://www.slac.stanford.edu/econf/C1307292/docs/submittedArxivFiles/1309.7035.pdf> [[INSPIRE](#)].
- [34] CAST collaboration, *New CAST limit on the axion-photon interaction*, *Nat. Phys.* **13** (2017) 584.